Supplementary Information (SI)

High selectivity for n-dodecane hydroisomerization over highly siliceous ZSM-22 with low Pt loading

Pengyu Niu[a,b], Hongjuan Xi[a], Jun Ren[c], Minggui Lin[a], Qiang Wang[a], Litao Jia[a], Bo Hou[a,*], and Debao Li[a,*]

[a] State Key Laboratory of Coal Conversion, Institute of Coal Chemistry, Chinese Academy of Sciences, Taiyuan 030001, People's Republic of China

[b] University of Chinese Academy of Sciences, Beijing 100049, People's Republic of China

[c] School of Chemical and Environmental Engineering, North University of China, Xueyuan Road 3, Taiyuan, 030051, China

* Corresponding Author

E-mail: houbo@sxicc.ac.cn.

dbli@sxicc.ac.cn.

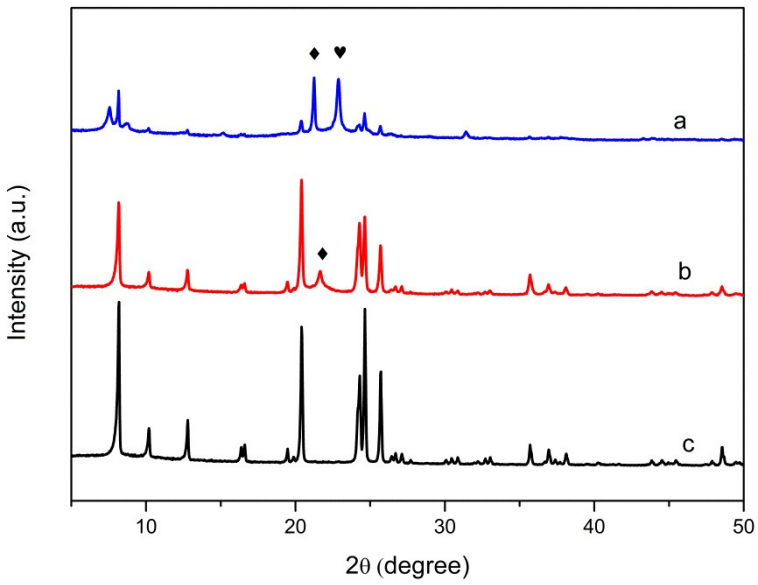

Figure S1. XRD patterns of samples obtained under different crystallization conditions. (a) crystallization without seeds at 160 °C, (b) crystallization with seeds at 160 °C, and (c) crystallization with seeds at 150 °C.

Figure S2 shows the XRD patterns of Z-40, Z-60, Z-100 and Z-Si. The relative intensity of diffraction peaks was enhanced with increasing of the Si/Al ratio. Strong peak at 24.65° was observed upon increasing of the Si/Al ratio, which became much stronger in siliceous ZSM-22. The differences are mainly caused by the difference in crystal growth where aluminum plays a significant role in the formation of ZSM-22 crystal[1].

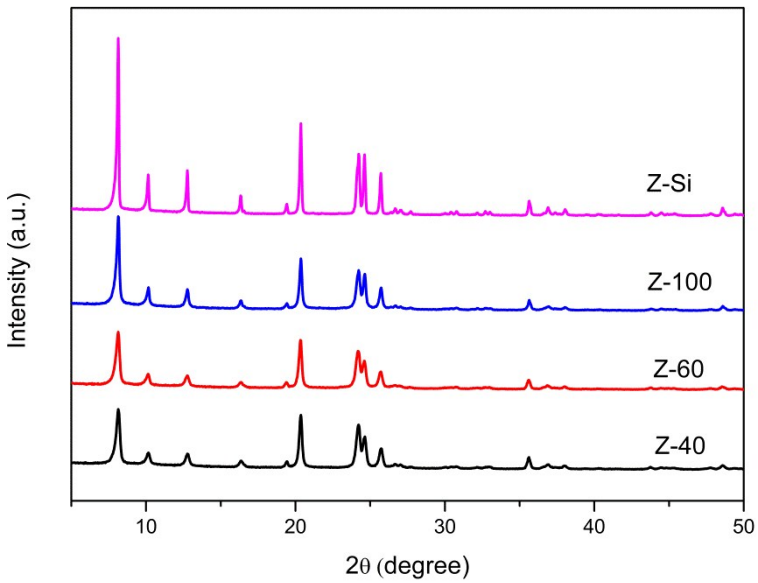

Figure S2. XRD patterns of Z-40, Z-60, Z-100 and Z-Si.

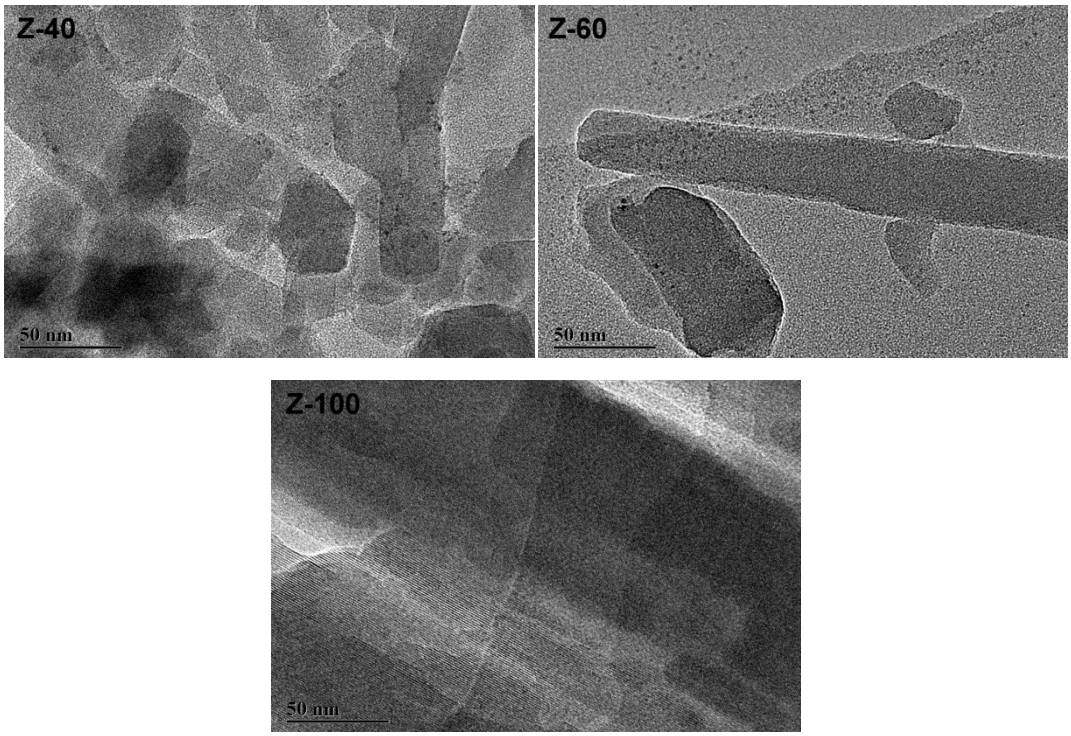

Figure S3. TEM images of Z-40, Z-60, and Z-100.

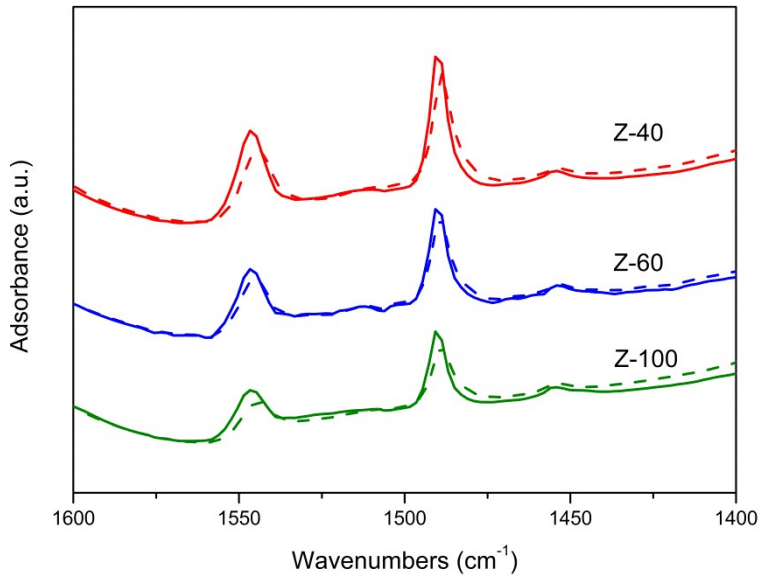

Figure S4. IR spectra of pyridine adsorbed on different samples at 200 °C (solid line) and 350 °C (dash line)

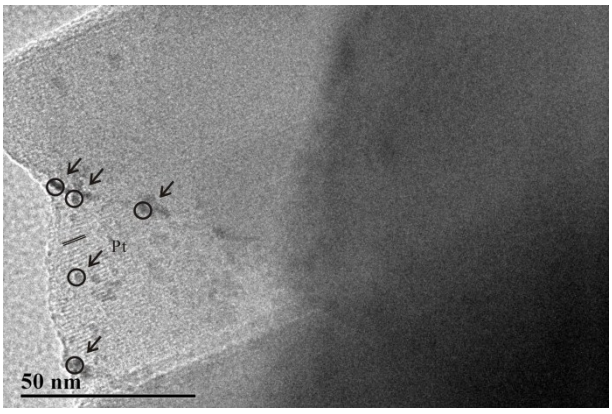

Figure S5. TEM image of Pt/Z-Si.

After HCl and alkaline solution treatment, the relative crystallinity and the textural properties of the two samples did not change obviously, shown in Figure S6 and S7. The textural properties of Z-Si, Z-Si-HCl and Z-Si-AT are listed in Table S1.

Both of Z-Si-HCl and Z-Si-AT were observed a weak signal centered at around -

103 ppm assigned to Q^3 environment, indicating the presence of defective sites. The presence of defective sites was also confirmed by $^1H^{29}Si$ CPMAS NMR spectrum of the two samples shown in Figure S8 (b). Structural defects (HO-Si-[$(OSi)_3$]) and ([HO]$_2$-Si-[$(OSi)_2$]) can be detected after alkaline solution treatment.

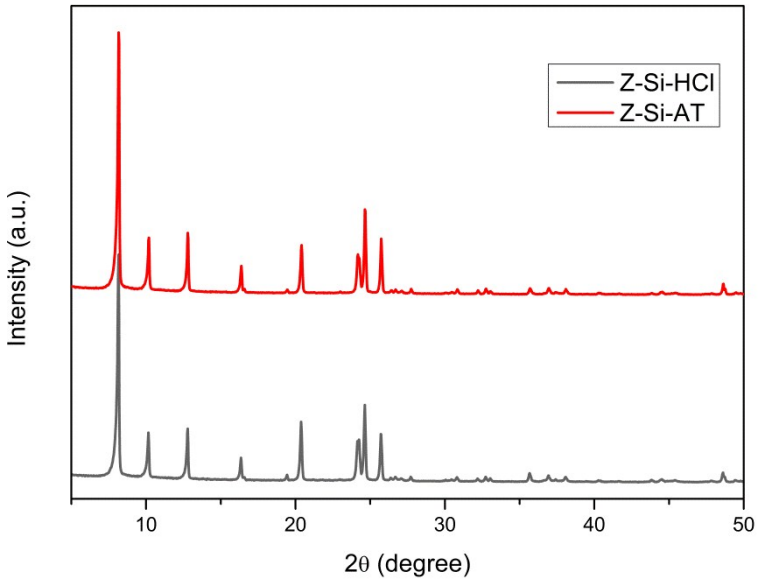

Figure S6. XRD patterns of Z-Si-HCl and Z-Si-AT.

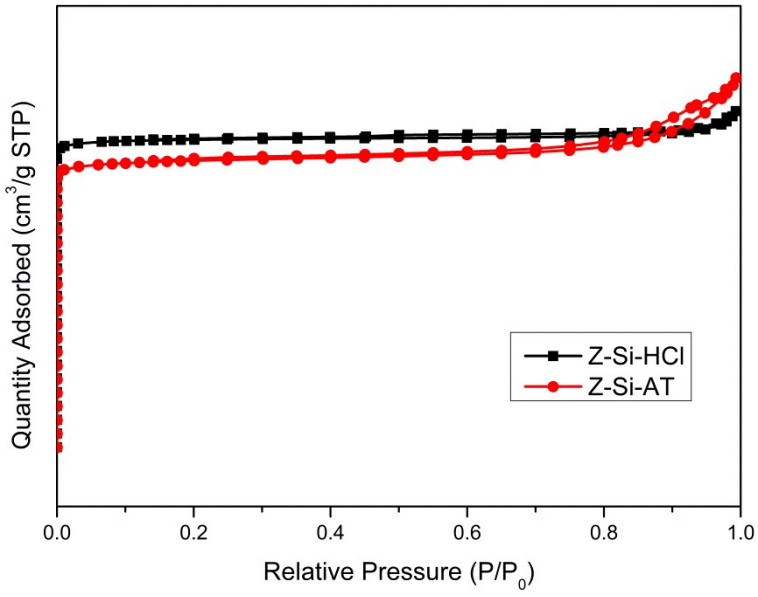

Figure S7. N_2 adsorption isotherms of Z-Si-HCl and Z-Si-AT.

Table S1. Textural characterization of Z-Si, Z-Si-HCl and Z-Si-AT

Samples	Si/Al[a]	S_{BET} (m^2g^{-1})	S_{micro} (m^2g^{-1})	S_{ext} (m^2g^{-1})	V_{micro} (cm^3g^{-1})	Brønsted acid (μmol g^{-1})
Z-Si	990	279	266	13	0.10	13
Z- Si-HCl	1344	293	287	6	0.10	7
Z-Si-AT	950	275	263	12	0.10	5

[a] Determined by ICP-OES.

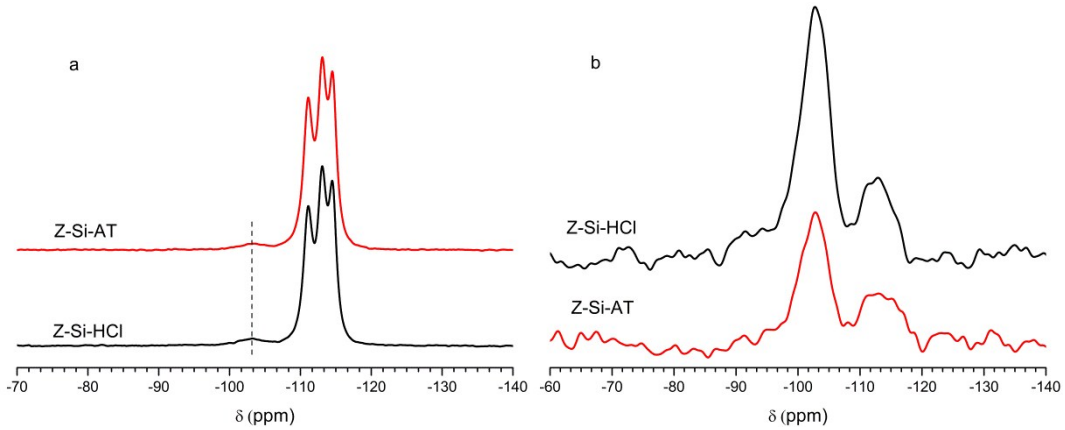

Figure S8. (a) ^{29}Si MAS NMR spectra and (b) $^{1}H^{29}Si$ CPMAS NMR spectrum of Z-Si-HCl and Z-Si-AT.

Table S2. CO chemisorption of Pt/Z-40 and Pt/Z-Si.

Catalysts	Pt dispersion (%)	Pt particle diameter (nm)
Pt/Z-40	53.57	2.11
Pt/Z-Si	20.51	5.52

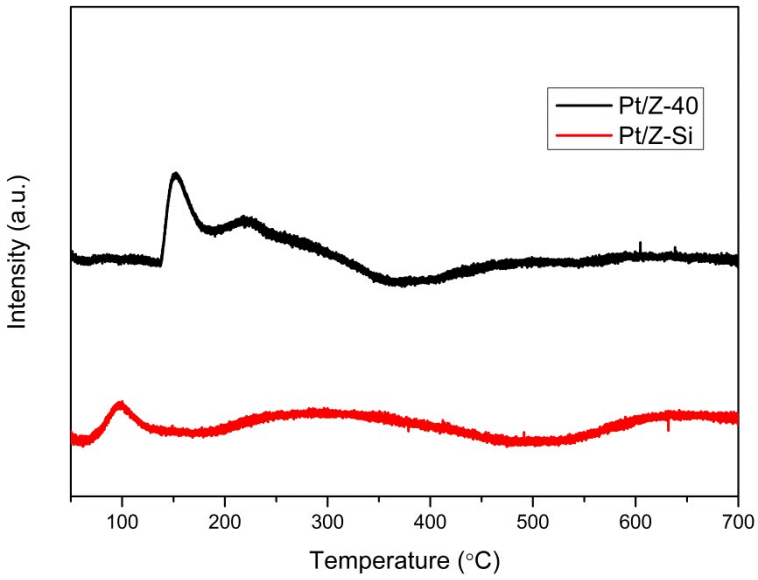

Figure S9. H_2 TPR spectra of the different samples.

The detailed mechanism for how linear alkenes are transformed into branched alkenes over acidic zeolites has also been extensively investigated by theoretical chemistry methods, which conclude that linear alkoxide intermediates formed upon adsorption are more stable than physisorbed linear alkenes. Moreover, the isomerization of a linear alkoxide into a branch alkoxide occurs via a protonated cyclopropane species as a transition state which is energetically favored compared to directly shifting the alkyl group.[2, 3] The mechanism for 1-octene hydroisomerization involves (i) 1-octene adsorption on the zeolite acid site to form physisorbed π-complex, (ii) and then to form a linear alkoxide species, (iii) isomerization of this linear alkoxide species into a branched alkoxide species, (iv) desorption of the branched alkoxide to form a mono-branched alkene and concurrent regeneration of the zeolitic acid site.

The basic steps for this mechanism have already been briefly outlined (see Figure 13).

The starting structure is a physisorbed π-complex, and then a linear alkoxide is formed via one step hydrogenation with a lower energy barrier 46.3 and 84.9 kJ/mol on silica-alumina and siliceous ZSM-22, respectively. This obtained a protonized molecule representing the first transition state (TS 1), shown in Figure S3. The next step starts from adsorbed alkoxide and forms an important configuration along the reaction energy path corresponds to a stable charged cyclopropane intermediate (see Figure S10), and this energy barrier is 78.2 and 137.0 kJ/mol on silica-alumina and siliceous ZSM-22, respectively. For the ring opening via the deprotonation of the cyclopropane configuration, the activation energy of 47.3 kJ/mol for silica-alumina ZSM-22 is obtained, which is lower than that of siliceous ZSM-22 with activation energy of 79.1 kJ/mol. The final reaction step is that the proton is transferred back to the acid site and binds to the C3 carbon atom, and C3-C4 carbon bond is broken to form branched alkoxide. The complete reaction pathway is depicted in Figure 13. The overall reaction, beginning from a physisorbed π-complex to a branched one, involves in total three transition states and two intermediates. The imaginary frequency of all transition states is listed in Table S3.

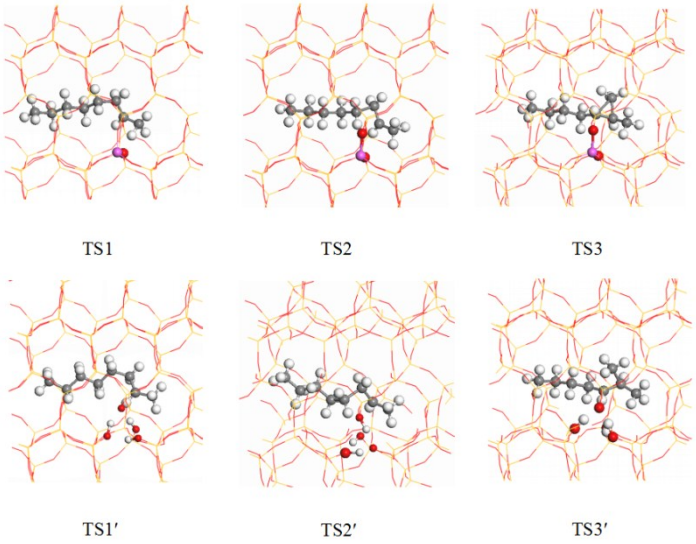

Figure S10. Transition state geometries (TS1-3 and TS1'-3') for catalytic isomerization of 1-ocene in silica-alumina and siliceous ZSM-22, respectively.

Table S3. The imaginary frequency of all transition states.

Transition state	imaginary frequency
TS1	212*i*
TS1'	189*i*
TS2	180*i*
TS2'	175*i*
TS3	162*i*
TS3'	207*i*

References

1. K. Hayasaka, D. Liang, W. Huybrechts, B. R. De Waele, K. J. Houthoofd, P. Eloy, E. M. Gaigneaux, G. van Tendeloo, J. W. Thybaut, G. B. Marin, J. F. M. Denayer, G. V. Baron, P. A. Jacobs, C. E. A. Kirschhock and J. A. Martens, *Chem.-Eur. J.*, 2007, **13**, 10070-10077.
2. T. Demuth, X. Rozanska, L. Benco, J. Hafner, R. A. van Santen and H. Toulhoat, *J. Catal.*, 2003, **214**, 68-77.
3. M. Boronat, P. Viruela and A. Corma, *Journal of Physical Chemistry*, 1996, **100**, 16514-16521.